

Modeling of Tunneling Spectroscopy in High- T_c Superconductors, Incorporating Band Structure, Gap Symmetry, Group Velocity, and Tunneling Directionality.

Z. Yusof, J.F. Zasadzinski, L. Coffey

*Science and Technology Center for Superconductivity,
Illinois Institute of Technology, Chicago Illinois 60616*

ABSTRACT

A theoretical model for tunneling spectroscopy employing tight-binding band structure, $d_{x^2-y^2}$ gap symmetry, group velocity, and tunneling directionality is studied. This is done to investigate if the model can exhibit the same wide range of characteristics observed in tunneling experiments on high- T_c superconductors. A band structure specific to optimally-doped $\text{Bi}_2\text{Sr}_2\text{CaCu}_2\text{O}_8$ (BSCCO) is used to calculate the tunneling density of states for a direct comparison to experimental tunneling conductance. A robust feature of the model is an asymmetric, decreasing conductance background, which is in agreement with experiment for BSCCO. The model also produces generally good agreement with the tunneling data especially in the gap region. In particular, the experimentally observed asymmetric conductance peaks can be understood with this model as a direct consequence of the $d_{x^2-y^2}$ gap symmetry. Dip features observed at $|eV| \sim 2\Delta$ in the experimental data are not found for any range of parameters in this model, indicating that these features are caused by other physical mechanisms such as strong coupling effects.

PACS numbers: 74.20. -z, 74.50. +r, 74.72. -h, 74.72. Hs

I. INTRODUCTION

Tunneling measurements on high- T_c superconductors (HTS) have revealed a rich variety of properties and characteristics. While tunneling spectroscopies on conventional superconductors can directly reveal the density of states (DOS) of the superconductor [1], the same measurements in HTS are not as easily interpreted. This is compounded by the lack of consensus on a single theory for the mechanism causing superconductivity in these materials. There are however, a set of characteristics that are consistently observed in a wide variety of tunneling measurements. These include : (i) variable sub-gap shape, ranging from sharp, cusp-like [2], to a flat, BCS-like feature [3] [4]; (ii) symmetric [2] [5] and asymmetric conductance peaks [3] [4] [6]; (iii) variable conductance shape outside the gap region (background), which can be flat, decreasing, or increasing values at high bias voltages [2] [4] [5] [7] [8] with varying degrees of asymmetry; (iv) dip features at $|eV| \sim 2\Delta$ [4] [5] [6].

Sometimes, a range of varying features can be seen using the same technique and on the same HTS sample. This is illustrated by the two $\text{Bi}_2\text{Sr}_2\text{CaCu}_2\text{O}_8$ (BSCCO) tunneling conductance curves shown in Fig. 1 [4]. These are superconductor-insulator-normal metal (SIN) conductance data obtained using the point-contact tunneling (PCT) method on the same optimally-doped BSCCO crystal. Fig. 1a shows a conductance curve with sharp, cusp-like sub-gap feature at zero-bias, and approximately symmetric conductance peaks as would be expected from a momentum-averaged $d_{x^2-y^2}$ (d-wave) DOS. On the other hand, the data shown in Fig. 1b has a much flatter, BCS-like sub-gap conductance, and a strongly asymmetric conductance peaks. Both conductance curves show distinctive dip features at $eV \sim -2\Delta$ and a decreasing, asymmetric background conductance outside the gap. The two curves of Fig. 1 display characteristics that are also seen in other tunneling data. Vacuum tunnel junction on BSCCO from scanning tunneling microscopy (STM) [4] [5] display gap features in between the two extremes of Figs. 1a and 1b and more symmetric dip features. It is apparent that data collected from identical samples using the same technique can yield a variety of tunneling conductance curves which may at first seem contradictory. Any model

that tries to explain superconductivity in HTS must be able to consistently account for these variable features observed in tunneling measurements.

It is found experimentally that the sharpest gap features are obtained when the high-bias background is weakly decreasing as shown in Fig. 1 [2] [4] [5]. A quantitative measure is the conductance peak height to background (PHB) ratio which is > 2 for both spectra of Fig. 1. When the background conductance is linearly increasing ($\propto |V|$), the PHB ratio is invariably much less than 2 [2]. This suggests that the linearly increasing background is arising from an additional conductance channel such as inelastic tunneling [9] [10].

Another indication that the decreasing background is an intrinsic effect of elastic tunneling in HTS is that it cannot be explained by any extrinsic processes such as junction heating, which might be a concern with local probes such as PCT or STM. PCT junctions on Nb [11] showed no evidence of heating whatsoever. Also, the heating power is V^2/R_J and considering a fixed voltage of say $V = 200$ meV, the effects of heating should scale with junction resistance R_J . The PCT junction of Fig. 1a has $R_J \sim 2$ k Ω whereas STM junctions are typically $10^9 \Omega$ [4] [5]. Yet both PCT and STM junctions show a similar decreasing background. It is unlikely that junction area alone would account for the factor of 10^6 difference in PCT and STM junctions (leading to fixed power/area) and therefore heating is ruled out as the explanation of decreasing background.

A standard technique in analyzing the tunneling conductance data in HTS is to use a smeared BCS function [12] in which a scattering rate parameter, Γ , is used to account for any broadening of the gap region in the DOS. This method of analysis suffers from the deficiency that it does not adequately treat the problem of a gap with d-wave symmetry, and it cannot explain the asymmetry observed in tunneling conductances. In addition, it also requires that the comparison be made with normalized tunneling conductance data. This is done by dividing the experimentally measured conductance by its “normal state” value which is usually obtained by extrapolating the high bias background conductance down to zero bias. However, since HTS tunneling conductance can exhibit varied and complex background shape, this procedure may “filter out” too much information from the conductance data.

This paper will deal with the problem of analyzing HTS conductance data from a different perspective. Rather than manipulating or normalizing the conductance data in order to fit the smeared BCS model, the experimental conductance data are left alone, and the model is adapted to match the experimental data. The model that will be presented has three general features: (i) a realistic band structure for the $Cu - O_2$ plane in HTS; (ii) a tunneling matrix element incorporating directionality and group velocity [13]; (iii) gap symmetry.

We will apply this model to optimally-doped BSCCO by using a band structure specific to this HTS obtained from angle-resolved photoemission spectroscopy (ARPES) [14]. Since there is an emerging consensus that the pairing interaction in HTS has a d-wave symmetry, the DOS calculated with this model will use this gap symmetry. This result will then be compared to the two different BSCCO data shown earlier. It is emphasized that this comparison is done with the *unnormalized* experimental data.

One of the early theoretical model calculations for the normal state and superconducting DOS of HTS was done by Fedro *et al.* [15] using the tight-binding band structure $\xi_{\mathbf{k}}$ including the next-nearest neighbor hopping (t - t' model) to describe the electrons in the $Cu - O_2$ planes [16]

$$\xi_{\mathbf{k}} = -2t[\cos(k_x a) + \cos(k_y a)] + 4t' \cos(k_x a) \cos(k_y a) - \mu$$

where t and t' are nearest-neighbor and next nearest-neighbor hopping energies respectively, and μ is the chemical potential. Both $\Delta = \Delta_o$ (s-wave) and d-wave gap symmetries were considered. The DOS with the s-wave gap symmetry showed the expected BCS-like gap shape with flat sub-gap feature, while the DOS with the d-wave gap symmetry showed a V-shaped, cusp-like feature at zero-bias. An interesting feature of this DOS calculation is the presence of as many as two singularities in the normal state. When $t' = \mu = 0$, there exists a van Hove singularity (VHS) in the center of the band (Fig. 1a of Ref. 15). This is due to the saddle-point in k -space near $(\pi, 0)$ in the band structure. For the hole-doped situation ($\mu < 0$), this singularity exists at an energy higher than the gap. When the t' term is considered, the VHS shifts to below the energy gap region of the DOS. There is also a

second singularity at the lower edge of the energy band (Fig. 1c and 1d of Ref. 15). This additional singularity is caused by the extra flattening-out of the energy band at $\mathbf{k} = (0, 0)$. However, other than the quasiparticle peaks at $eV = \pm\Delta$, no HTS tunneling measurement has displayed any other peaks in the DOS as prominent and distinctive as those shown in the t - t' model DOS calculation of Ref. 15. Fig. 1a, which is a typical curve for BSCCO, shows no direct evidence of a VHS either inside or outside the gap.

It was proposed by Harrison [13] that tunneling measurements are insensitive to band structure effects. Although the tunneling matrix element is usually considered to be constant in the conventional treatment of tunneling, a more careful consideration of the matrix element reveals a need for a factor $\nabla\xi_{\mathbf{k}}$ (which is proportional to the particles' group velocity v_g and thus will be called as such) and directionality in the tunneling matrix element [17], since quasiparticles with momentum perpendicular to the barrier interface have the highest probability of tunneling. For the particular case where electrons normal to the barrier are the *only* ones which tunnel, there is an exact cancellation of the one-dimensional band structure DOS by the group velocity.

As shown by Kouznetsov *et al.* [9], the inclusion of the group velocity and directionality to the t - t' model removes the extraneous singularities from the calculated DOS. A varying background shape outside the energy gap region can also be obtained by varying the tunneling direction. Moreover, a d-wave gap symmetry may also produce a sub-gap structure that is flat or s-wave like. The theoretical model used in this paper develops this line of approach further with the added refinement of using a band structure specific to optimally-doped BSCCO.

II. THEORETICAL MODEL

The tunneling DOS of a superconductor is determined by the imaginary part of the single-particle Green's function,

$$N(E) = -\frac{1}{\pi} \text{Im} \sum_{\mathbf{k}} |T_{\mathbf{k}}|^2 G(\mathbf{k}, E) \quad (1)$$

For the superconducting state,

$$G(\mathbf{k}, E) = \frac{u_k^2}{E - E_k + i\Gamma} + \frac{v_k^2}{E + E_k + i\Gamma}$$

where u_k^2 and v_k^2 are the usual coherence factors, Γ is the quasiparticle lifetime broadening factor, and $E_k = \sqrt{|\Delta(\mathbf{k})|^2 + \xi_{\mathbf{k}}^2}$ with the gap function for d-wave symmetry $\Delta(\mathbf{k}) = \Delta_o[\cos(k_x a) - \cos(k_y a)]/2$. The tunneling matrix element $|T_{\mathbf{k}}|^2$ is written as

$$|T_{\mathbf{k}}|^2 = v_g D(\mathbf{k})$$

where v_g is the group velocity defined as $v_g = |\nabla_{\mathbf{k}} \xi_{\mathbf{k}} \cdot \mathbf{n}|$ and $D(\mathbf{k})$ is the directionality function that has the form [18],

$$D(k) = \exp \left[-\frac{k^2 - (\mathbf{k} \cdot \mathbf{n})^2}{(\mathbf{k} \cdot \mathbf{n})^2 \theta_o^2} \right] \quad (2)$$

The unit vector \mathbf{n} defines the tunneling direction, which is perpendicular to the plane of the junction, whereas θ_o corresponds to the angular spread in k -space of the quasiparticle momenta with non-negligible tunneling probability with respect to \mathbf{n} . This is shown schematically in Fig. 2 for a quadrant of the Brillouin zone, where both the Fermi surface (dashed line) and the d-wave gap are indicated. The thick solid straight line in Fig. 2 indicates the most probable tunneling direction defined by an angle θ with respect to the k_x direction. The thin straight lines indicate the angular spread of tunneling given by θ_o . This means that for $\theta_o \ll 1$, only quasiparticles with momenta extremely close to the direction of \mathbf{n} have significant tunneling probability.. It should be mentioned that this tunneling model does not take into account the possibility of an energy dependent barrier strength [19], which may or may not appreciably affect $|T_{\mathbf{k}}|^2$ [20]. Such barrier effects become appreciable when the tunneling particle energy is comparable to the barrier height. The focus of our analysis is the gap region where these effects are assumed to be small.

Another effect which is not included in the model is the zero-bias conductance peak (ZBCP) which is sometimes observed in certain HTS tunneling. As Fig. 1 clearly shows, there is no evidence of any ZBCP in the SIN tunneling conductance data of BSCCO either from PCT [2] [4] or from STM [4] [5]. Recent theoretical work [21] [22] [23] [24] [25] [26] on the effects of interface scattering by quasiparticles predicts that a d-wave anisotropic gap should be suppressed to zero at a tunneling interface. A redistribution of the quasiparticle spectral weight for states in the vicinity of the interface as a result of this suppression of the gap will result in a zero energy peak in the spectral weight. This is predicted to result in a ZBCP in the local DOS. Furthermore, a sharp upturn in the temperature dependence of the critical current at low temperatures is another consequence of the predicted ZBCP [26]. Some tunneling measurements have shown the presence of zero-bias anomalies but these may be explainable in terms of Josephson currents due to weak links [27]. Most tunneling measurements on SIN junctions do not reveal the presence of the ZBCP with one exception being certain tunneling measurements on YBaCuO junctions [28] [29]. Moreover, a survey of critical current measurements [30] does not show the predicted sharp upturns in the low temperature behavior of critical currents in a wide variety of Josephson junctions. These observations suggest that more work is required to relate the effects of interface scattering to experimental measurements and that the role of interface scattering and accompanying gap suppression is unclear at present. Hence, we have not included these predicted consequences of interface scattering in the present work.

At this point, the theoretical model will focus on the case of optimally-doped BSCCO. We use the effective band structure extracted from ARPES [14],

$$\begin{aligned} \xi_k = & c_o + \frac{1}{2}c_1[\cos(k_x a) + \cos(k_y a)] + c_2 \cos(k_x a) \cos(k_y a) + \frac{1}{2}c_3[\cos(2k_x a) + \cos(2k_y a)] \\ & + \frac{1}{2}c_4[\cos(2k_x a) \cos(k_y a) + \cos(k_x a) \cos(2k_y a)] + c_5 \cos(2k_x a) \cos(2k_y a) \end{aligned} \quad (3)$$

where the phenomenological parameters are $c_o = 0.1305$, $c_1 = -0.5951$, $c_2 = 0.1636$, $c_3 = -0.0519$, $c_4 = -0.1117$, $c_5 = 0.0510$. Part of the Fermi surface from this band structure is shown as the dashed curve in Fig. 1.

III. RESULTS

The shape of the “normal-state” DOS is examined first by setting $\Delta_o = 0$ and imposing no directionality (similar to Fig. 1c in Ref. 15). This case may be realized experimentally in PCT by having the tunnel current flow radially outward from the tip into all possible \mathbf{k} states of the $Cu - O_2$ plane. Implied here is a subsequent c-axis transport process to complete the current flow through the crystal. Fig. 3a shows the DOS of the full energy band for three different Γ values without any group velocity effects. This, combined with no directionality, is equivalent to setting $|T_{\mathbf{k}}|^2 = 1$ in Eq. 1. The VHS is located ~ 34 meV below the Fermi energy for $\Gamma = 0.003$ eV and its location shifts slightly towards higher energy as Γ increases. The most obvious difference between the band structure of Eq. 3 and the t - t' model of Ref. 15 is the absence of the second singularity at the lower band edge. When v_g is factored in while maintaining no directionality, significant changes are observed (Fig. 3b). The VHSs are no longer as distinctive as before, with peaks in the DOS having smaller amplitudes (no rescaling of the numerical data were done in Fig. 3a and 3b). There is also a clearer shift towards higher energies in the location of the highest peak in the DOS as Γ increases. Additionally, the model DOS also produces a slightly asymmetric, decreasing background at large $|E|$. In contrast to the one-dimensional tunneling model of Harrison [13] (more appropriate for planar junctions), there is no complete cancellation of the band structure effects by the group velocity. However, there is clearly a strong reduction of the VHS. Note that the group velocity is entering as a scalar quantity.

Under identical circumstances as described for Fig. 3 ($|T_k|^2 = 1$ in Eq. 1), the DOS for $\Gamma = 0.003$ eV is examined with the inclusion of the d-wave gap (Fig. 4). The DOS in Fig. 4a, which does not include v_g , shows three distinctive peaks. The leftmost peak, which is also the highest, is the VHS, while the remaining two are the quasiparticle peaks. The weak “mirror image” of the VHS at positive energy is a consequence of the non-zero Γ value. As is evident in Fig. 1, the VHS is not seen in the BSCCO data. With the inclusion of v_g , the presence of the VHS is barely noticeable (Fig. 4b), suggesting that group velocity effects

are playing an important role in HTS tunneling. Even though both DOS exhibit the sharp, cusp-like gap feature, there is an observable difference in the shape of the sub-gap region. The inclusion of v_g produces a tunneling DOS which has less curvature and a more linear, V-shaped feature near zero bias.

The model DOS is compared directly with the BSCCO tunneling data of Fig. 1a, as shown in Fig. 5. The DOS calculated with and without v_g show a weakly decreasing background outside the gap region. The shape inside the gap seems to agree exceedingly well with the DOS calculated without using v_g as shown in Fig. 5a. However, the extraneous presence of the VHS in the model cannot be reconciled with the experimental data. On the other hand, the DOS calculated with v_g in Fig. 5b shows a better overall agreement, especially in matching the slight asymmetry of the quasiparticle peaks in addition to the obvious absence of the VHS. The model in both cases produces a weakly decreasing background for $|eV| > \Delta$ that is similar to the experimental data. The cusp-like shape of the gap in the data and the close agreement with this model suggests the possibility that this BSCCO data is a result of a tunneling process with a very weak directionality. This allows for quasiparticles with all momentum directions to be involved in the tunneling process, which is a possible scenario if the tip in the PCT is partly imbedded in the sample.

The second BSCCO data (shown in Fig. 1b and more clearly in Fig. 6) presents features not observed in the data of Fig. 5. There are asymmetric quasiparticle peaks, with the higher peak in the negative bias voltage (filled states). This asymmetry is also seen in STM data on the same BSCCO crystal [4]. Furthermore, the sub-gap region shows a flatter, BCS-like feature. A smeared BCS fit of this data from Ref. 4 showed a reasonable agreement in the sub-gap region, but could not account for the asymmetric peaks and shape of the conductance at $|eV| > \Delta$. It is clear that for a gap with d-wave symmetry, a flat sub-gap tunneling DOS can only be obtained with a strong directionality effect. Also, since the voltage of the conductance peaks is the same in Figs. 1a and 1b, it implies that the preferred tunneling direction is near the lobe of the d-wave gap.

For this data, the full model is used, employing v_g and the directionality function of

Eq. 2. As can be seen in Fig. 6a, there is excellent agreement with the experimental data around the gap region up to $|eV| \sim 60$ meV, displaying the same degree of asymmetry and an almost flat sub-gap structure. The value of Δ_o used in this model (46 meV) is larger than that found using the smeared BCS fit (38 meV in Ref. 4 and 27.5 meV in Ref. 5). The model DOS has a large drop in the positive bias side beyond the gap. This is due to the fact that since the directionality angle in Eq. 2 is small with \mathbf{n} almost along the k_x -axis and close to $(\pi, 0)$, the number of states above the Fermi surface falls off rapidly as one approaches the edge of the Brillouin zone. As θ_o (which controls the width or angular spread in $D(k)$) increases while keeping θ constant, there are not only more empty states, but also higher energy states above the Fermi surface being summed in Eq. 1. This explains why there are more DOS in the higher energy range in Fig. 6d. In addition, Fig. 6 also shows that the increase in θ_o also changes the shape of the sub-gap structure dramatically, approaching the V-shaped feature found earlier. The larger θ_o signifies a weaker tunneling directionality, and the V-shape arises from the inclusion of \mathbf{k} states near the line of nodes along (π, π) .

A natural question leading off from this is why not perform the DOS calculation at a larger θ to include more empty and higher energy states so as to eliminate the large DOS drop-off in the model at positive bias? There are two major reasons why this is not done. As θ increases towards $\pi/4$, the tunneling direction approaches the node of the d-wave gap symmetry. This means that the value of Δ_o in the model has to be set at a higher, unrealistic value for this HTS compound to be able to match the position of the quasiparticle peaks in the tunneling data. Secondly, the smaller θ is chosen to take advantage of the influence of the band edge on the asymmetry of the quasiparticle peaks. As the tunneling direction approaches $(\pi, 0)$, the asymmetry of the peaks is maximized.

Hence, the value of θ that is used in Fig. 6 is not chosen arbitrarily, but rather it is the angle which gives the appropriate degree of asymmetry to match the experimental data. However, note that even as θ_o is increased, the degree of asymmetry of the quasiparticle peaks of the model has not been altered as significantly as the other features such as the decreasing asymmetry of the conductance outside the gap. This suggests that the quasi-

particle peak asymmetry is primarily a consequence of the d-wave order parameter. Two further investigations are done to confirm this. In Fig. 7, the same experimental BSCCO conductance data as in Fig. 6 is compared to the model using the isotropic s-wave gap $\Delta=\Delta_o$. In this case, the model conductance peaks tend to be more symmetric, and the slight asymmetry here can be attributed to the band edge effect as shown by the normal state curve (dashed line). Secondly, we perform the model calculation for both s- and d-wave gap symmetries at a large θ (0.4 rad) in Eq. 2. This generates an asymmetric, normal state background which increases towards large, positive E . As can be seen in Fig. 8, even with this kind of normal state behavior, the d-wave DOS (solid line) still shows quasiparticle peaks asymmetry that is higher in the negative voltage side (filled states), although the degree of asymmetry is less than that in Fig. 6. The s-wave DOS, on the other hand, still tends to have more symmetrical quasiparticle peaks, and the minor asymmetry seems to correspond to the shape of the underlying normal state conductance.

The origin of the asymmetry of the peaks in the tunneling DOS can be studied further by considering the role of the tunneling matrix element $|T_{\mathbf{k}}|^2$ in the clean limit case ($\Gamma = 0$) where

$$N(E) = \sum_{\mathbf{k}} |T_{\mathbf{k}}|^2 \left[\frac{1}{2}(1 + \xi_{\mathbf{k}}/E_{\mathbf{k}})\delta(E_{\mathbf{k}} - E) + \frac{1}{2}(1 - \xi_{\mathbf{k}}/E_{\mathbf{k}})\delta(E_{\mathbf{k}} + E) \right] \quad (4)$$

For positive bias voltages ($E \geq 0$), the first term, involving the coherence factor $\frac{1}{2}(1+\xi_{\mathbf{k}}/E_{\mathbf{k}})$, contributes to the density of states because of the delta function $\delta(E_{\mathbf{k}} - E)$. In this case, the tunneling matrix element $|T_{\mathbf{k}}|^2$ selects only a relatively short region of states in k -space in which the coherence factor is greater than unity. For the majority of states integrated over (as seen in Fig. 2) in the calculation of $N(E)$, the coherence factor is less than unity, in fact dropping to zero at the origin for a d-wave symmetry superconducting state.

For negative bias voltages ($E \leq 0$), the second term, involving the coherence factor $\frac{1}{2}(1 - \xi_{\mathbf{k}}/E_{\mathbf{k}})$, contributes to the density of states because of the delta function $\delta(E_{\mathbf{k}} + E)$. In this case however, the tunneling matrix element selects out a larger region of k -states where the coherence factor is greater than unity. These are states below the Fermi surface

in Fig. 2. The overall effect then is to have a larger negative bias conductance compared to the positive bias part of the conductance. This asymmetry is greater for d-wave than for s-wave because, in the latter case, the superconducting gap does not decrease in magnitude and become zero at $\mathbf{k} = 0$. For the positive bias voltage case, this tendency feature of $\Delta_{\mathbf{k}} = 0$ at $\mathbf{k} = 0$ enhances the reduction of the overall magnitude of the positive bias voltage $N(E)$ for the d-wave case, as has just been pointed out.

Therefore, the underlying asymmetry in this model is primarily due to the d-wave gap symmetry. The proximity of the quasiparticle gap to the band edge in Fig. 6 simply enhances the degree of asymmetry of the peaks. Also note that in Fig. 8, there are more higher energy DOS than shown in Fig. 6 since θ is larger. However, as argued earlier, the value of Δ_o for the d-wave DOS is also considerably larger (75 meV) to be able to produce roughly the same peak-to-peak gap value since the tunneling direction \mathbf{n} in Eq. 2 is now closer to the node of the d-wave gap.

The lack of agreement between the model and the data in Fig. 6 for $V > 0$ outside the gap is a significant deficiency of the model used here. There are several possible explanations for this. The band structure for BSCCO that was obtained from the phenomenological fit of ARPES data may be inadequate. This is because ARPES experiments only yield reliable information for electron emission ($V < 0$) and thus only probe the filled states of the DOS. Next is the possibility of an additional conductance channel, such as inelastic tunneling, which has been shown to also produce the dip feature seen in the tunneling data [9] and an increasing background conductance [9] [10]. There is also the possibility of another energy band close to the top of the band which allows for additional tunneling states.

In summary, this model presents a significant improvement over the use of a smeared s-wave model for the DOS in analyzing tunneling conductance data in HTS. The model makes use of a tunneling matrix element that incorporates the group velocity of carriers, and tunneling directionality. With a band structure which has been used previously to analyze ARPES measurement on optimally-doped BSCCO, the model is able to duplicate the wide range of features seen in the experimental tunneling measurements on this compound.

These features include the asymmetric quasiparticle conductance peaks in the superconducting state, variable sub-gap conductance behavior, and the absence of normal state band structure features, in particular the VHS. The asymmetry of the experimentally measured quasiparticle conductance peaks, which can be duplicated in the model using the d-wave superconducting gap, may be a signature of the d-wave gap symmetry in BSCCO. Under no circumstances did the model exhibit the dip features at $|eV| \sim 2\Delta$ that are consistently observed experimentally. This indicates that the dip features arise from some other process such as strong coupling effects [4] or an additional conductance channel such as inelastic tunneling [9].

The authors are grateful to Nobuaki Miyakawa for providing the experimental data. This work was partially supported by the U.S. Department of Energy, Division of Basic Energy Sciences - Material Sciences under contract No. W-31-109-ENG-38, and the National Science Foundation, Office of Science and Technology Centers under contract No. DMR 91-20000. ZY acknowledges support from Division of Educational Programs, Argonne National Laboratory.

REFERENCES

- [1] E.L. Wolf, *Principles of Electron Tunneling Spectroscopy* (Oxford Univ. Press, New York, 1985).
- [2] J.F. Zasadzinski, L. Ozyuzer, Z. Yusof, J. Chen, K.E. Gray, M. Mogilevsky, D.G. Hinks, J.L. Cobb, J.T. Market, *Spectroscopic Studies of High T_c Cuprates*, ed. I. Bozovic, D. van der Marel, Proc. SPIE 2696, 338 (1996) (Bellingham).
- [3] J. Chen, J.F. Zasadzinski, K.E. Gray, J.L. Wagner, D.G. Hinks, *Phys. Rev. B* **49**, 3683 (1994).
- [4] Y. DeWilde, N. Miyakawa, P. Guptasarma, M. Ivarone, L. Ozyuzer, J.F. Zasadzinski, P. Romano, D.G. Hinks, C. Kendziora, G.W. Crabtree, K.E. Gray, (preprint). N. Miyakawa *et al.*, (unpublished).
- [5] C. Renner, O. Fischer, *Phys. Rev. B* **51**, 9208 (1995).
- [6] H. Hancotte, R. Deltour, D.N. Davydov, A.G.M. Jansen, P. Wyder, *Phys. Rev. B* **55**, R3410 (1997).
- [7] Q. Huang, J.F. Zasadzinski, K.E. Gray, E.D. Bukowski, D.M. Ginsberg, *Physica C* **161**, 141 (1989).
- [8] For a review, see T. Hasegawa, H. Ikuta, K. Kitasawa, *Physical Properties of High Temperature Superconductors III*, ed. D.M. Ginsberg (World Scientific, Singapore, 1992).
- [9] K. Kouznetsov, L. Coffey, *Phys. Rev. B* **54**, 3617 (1996).
- [10] J.R. Kirtley, D.J. Scalapino, *Phys. Rev. Lett.* **65**, 798 (1990).
- [11] Q. Huang, J.F. Zasadzinski, K.E. Gray, *Phys. Rev. B* **42**, 7953 (1990).
- [12] R.C. Dynes, V. Narayanamurti, J.P. Garno, *Phys. Rev. Lett.* **41**, 1509 (1978).

- [13] W.A. Harrison, *Phys. Rev.* **123**, 85 (1961).
- [14] M.R. Norman, M. Randeria, H. Ding, J.C. Campuzano, *Phys. Rev. B* **52**, 615 (1995).
- [15] A.J. Fedro, D.D. Koelling, *Phys. Rev. B* **47**, 14342 (1993).
- [16] Here we have assumed that the crystal has tetragonal symmetry.
- [17] G. Beuermann, *Z. Phys. B* **44**, 29 (1981).
- [18] M. Ledvij, R.A. Klemm, *Phys. Rev. B* **51**, 3269 (1995).
- [19] J.Y.T. Wei, C.C. Tsuei, P.J.M. van Bentum, Q. Xiong, C.W. Chu, M.K. Wu, (preprint).
- [20] For a discussion of models for the tunneling matrix element, including group velocity and directionality related issues, see C.B. Duke, *Tunneling in Solids, Solid State Physics*, Suppl. Vol. 10 (Academic Press, 1969); sect. 7(b) p. 54/55; sect. 18 p. 218/219.
- [21] Y.S. Barash, A.A. Svidzinsky, H. Burkhardt, *Phys. Rev. B* **55**, 15282 (1997).
- [22] W. Zhang, *Phys. Rev. B* **52**, 12538 (1995).
- [23] W. Widder, L. Bauernfeind, H.F. Braun, H. Burkhardt, D. Rainer, M. Bauer, H. Kinder, *Phys. Rev. B* **55**, 1254 (1997).
- [24] Y. Tanaka, S. Kashiwaya, *Phys. Rev. Lett.* **74**, 3451 (1995).
- [25] L.J. Buchholtz, M. Palumbo, D. Rainer, J.A. Sauls, *J. Low Temp. Phys.* **101**, 1099 (1995).
- [26] Y.S. Barash, H. Burkhardt, D. Rainer, *Phys. Rev. Lett.* **77**, 4070 (1996).
- [27] H. Srikanth, A.K. Raychaudhuri, *Physica C* **190**, 229 (1992).
- [28] S. Kashiwaya, Y. Tanaka, M. Koyanagi, H. Takashima, K. Kajimura, *Phys. Rev. B* **51**, 1350 (1995).
- [29] M. Covington, M. Aprili, E. Paraoanu, L.H. Greene, F. Xu, J. Zhu, C.A. Mirkin, *Phys. Rev. Lett.* **79**, 277 (1997).

[30] K.A. Delin, A.W. Kleinsasser, *Supercond. Sci. Technol.* **9**, 227 (1996).

FIGURE CAPTIONS

Fig. 1 : PCT SIN tunneling conductance data for optimally-doped BSCCO. Here, V is the sample voltage with respect to the tip.

Fig. 2 : A quadrant in k -space showing the partial lobes of the d-wave gap symmetry (solid curve), the line of directional tunneling (dark straight line), and the angular spread θ_o indicated schematically by the thin straight lines. The dashed curve represents part of the Fermi surface specific to optimally-doped BSCCO from Ref.14.

Fig. 3 : Normal state DOS calculation ($\Delta_o = 0$) showing the full band width for three Γ values. The dotted line is for $\Gamma = 0.003\text{eV}$, solid line is for $\Gamma = 0.008\text{ eV}$, and the dashed line is for $\Gamma = 0.08\text{ eV}$. (a) The DOS with no v_g and no directionality. The single prominent peak for each curve is the van Hove singularity. (b) The change in normal state DOS when v_g is included.

Fig. 4 : Numerical calculation of quasiparticle DOS with a d-wave gap symmetry. (a) The DOS with no v_g and no directionality. (b) DOS when v_g is included. The VHS is effectively unobservable in this case.

Fig. 5 : A comparison of the model (solid line) with BSCCO data from Fig. 1a (open circles). (a) $\Delta_o = 0.043\text{ eV}$, $\Gamma = 0.002\text{ eV}$, no v_g , no directionality. (b) $\Delta_o = 0.043\text{ eV}$, $\Gamma = 0.001\text{ eV}$, v_g present, no directionality. In each graph, the magnitude of the model DOS was divided by a constant value to show a clearer match with the experimental data. Γ is different in each case to produce the best fit to the data.

Fig. 6 : Comparison of model DOS (solid line) which includes v_g and directionality, with BSCCO SIN tunneling conductance data from Fig. 1b (open circles). Here $\Delta_o = 0.046\text{ eV}$, $\Gamma = 0.003\text{ eV}$, and $\theta = 0.25\text{ rad.}$ for all four numerical curves. All the values of θ_o shown are in radians. As in Fig. 5, each of the model DOS has been rescaled by a constant value.

Fig. 7 : Comparison of the same BSCCO data as in Fig. 5 (open circles) with the model using the isotropic s-wave gap symmetry $\Delta = \Delta_o$ (solid line). Here, $\Delta_o = 0.038\text{ eV}$,

$\Gamma = 0.0035$ eV, $\theta = 0.25$ rad, $\theta_o = 0.05$ rad to produce the best fit to the experimental data. The dashed line is the normal state ($\Delta_o = 0$).

Fig. 8 : Model DOS calculations for d-wave (solid line, $\Delta_o = 0.075$ eV), s-wave (dotted line, $\Delta_o = 0.040$ eV), and normal state (dashed line, $\Delta_o = 0$). All three DOS are calculated using parameters: $\Gamma = 0.002$ eV, $\theta = 0.4$ rad, $\theta_o = 0.02$ rad.

Fig 1

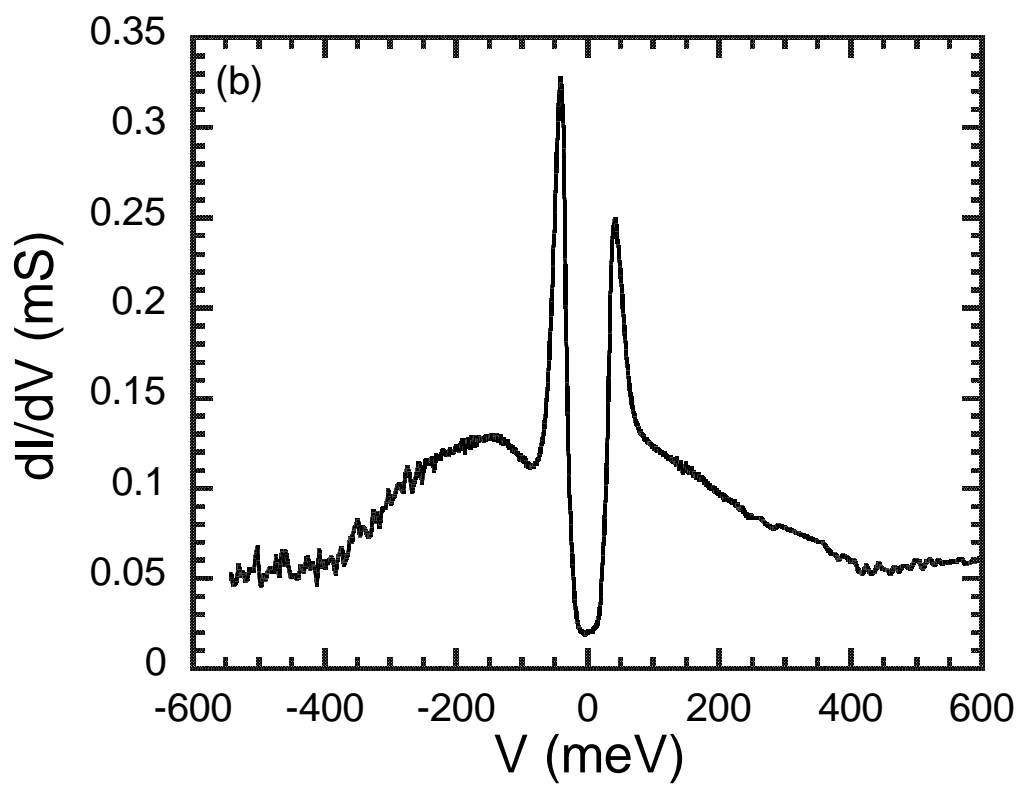
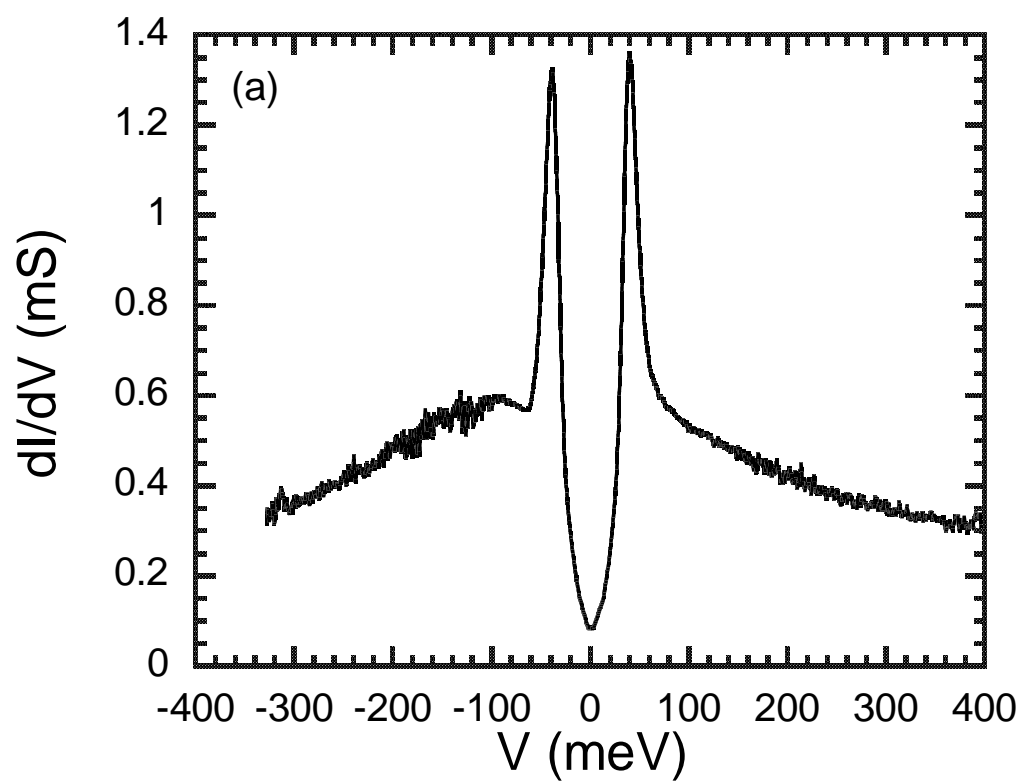


Fig. 2

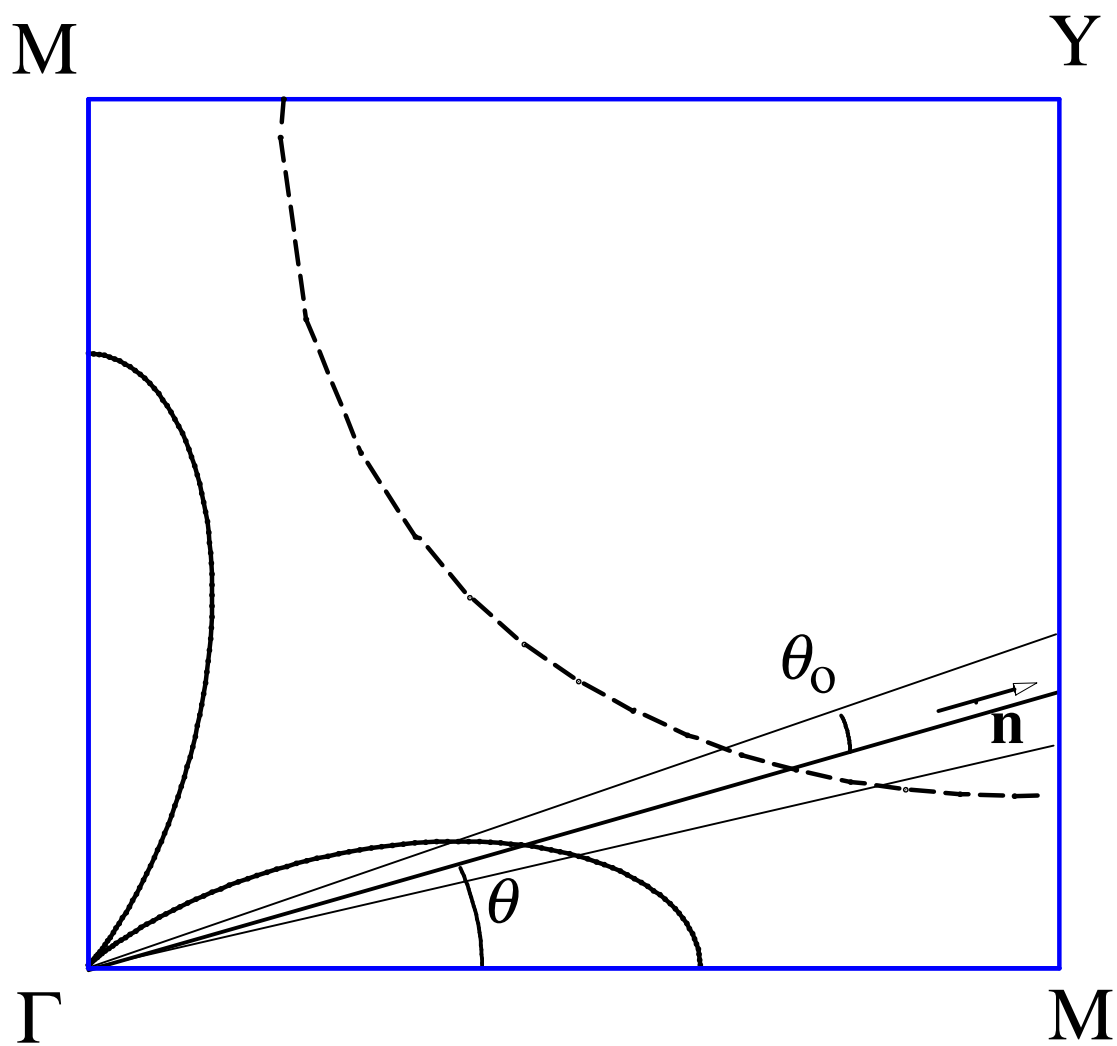


Fig. 3

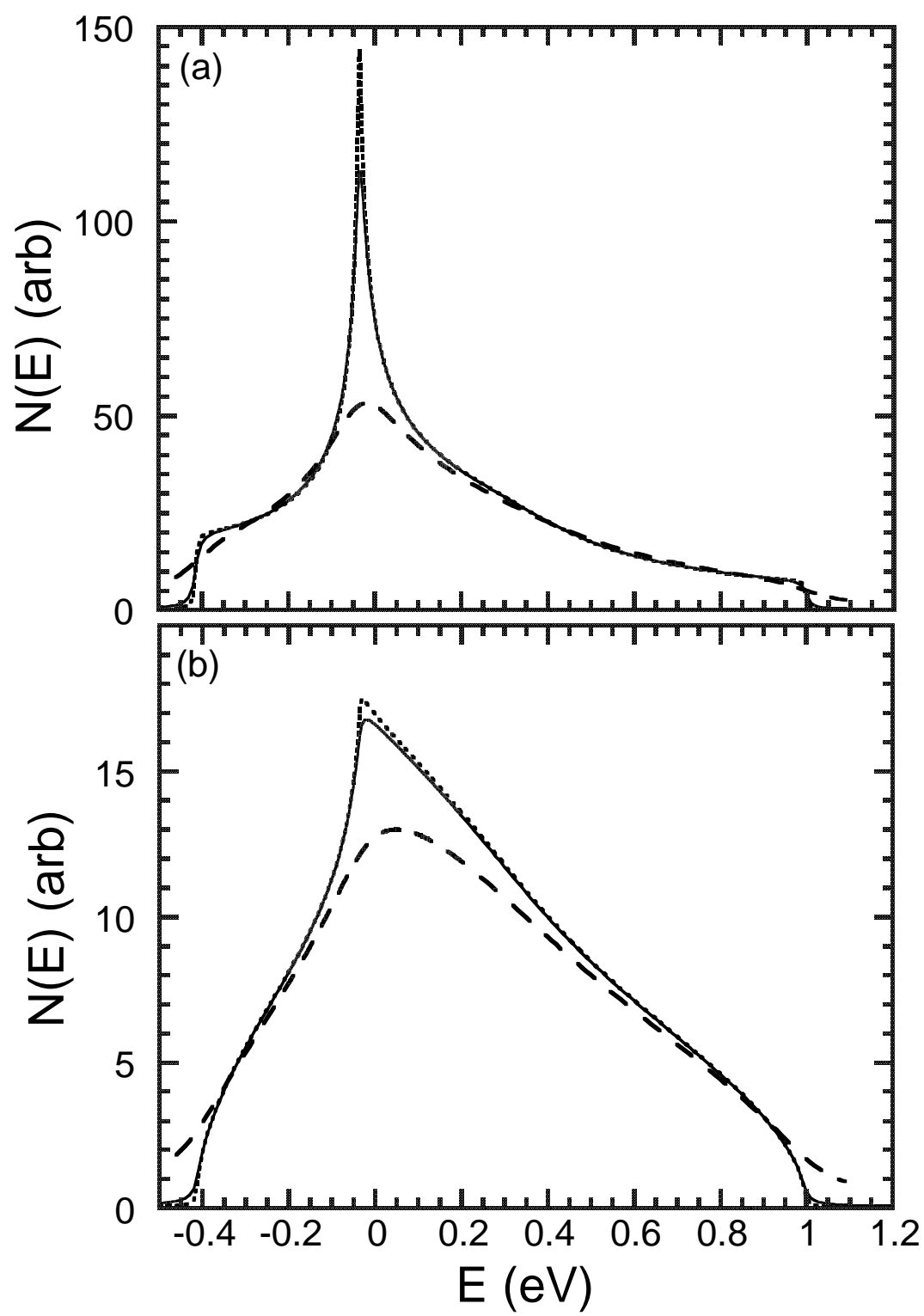


Fig. 4

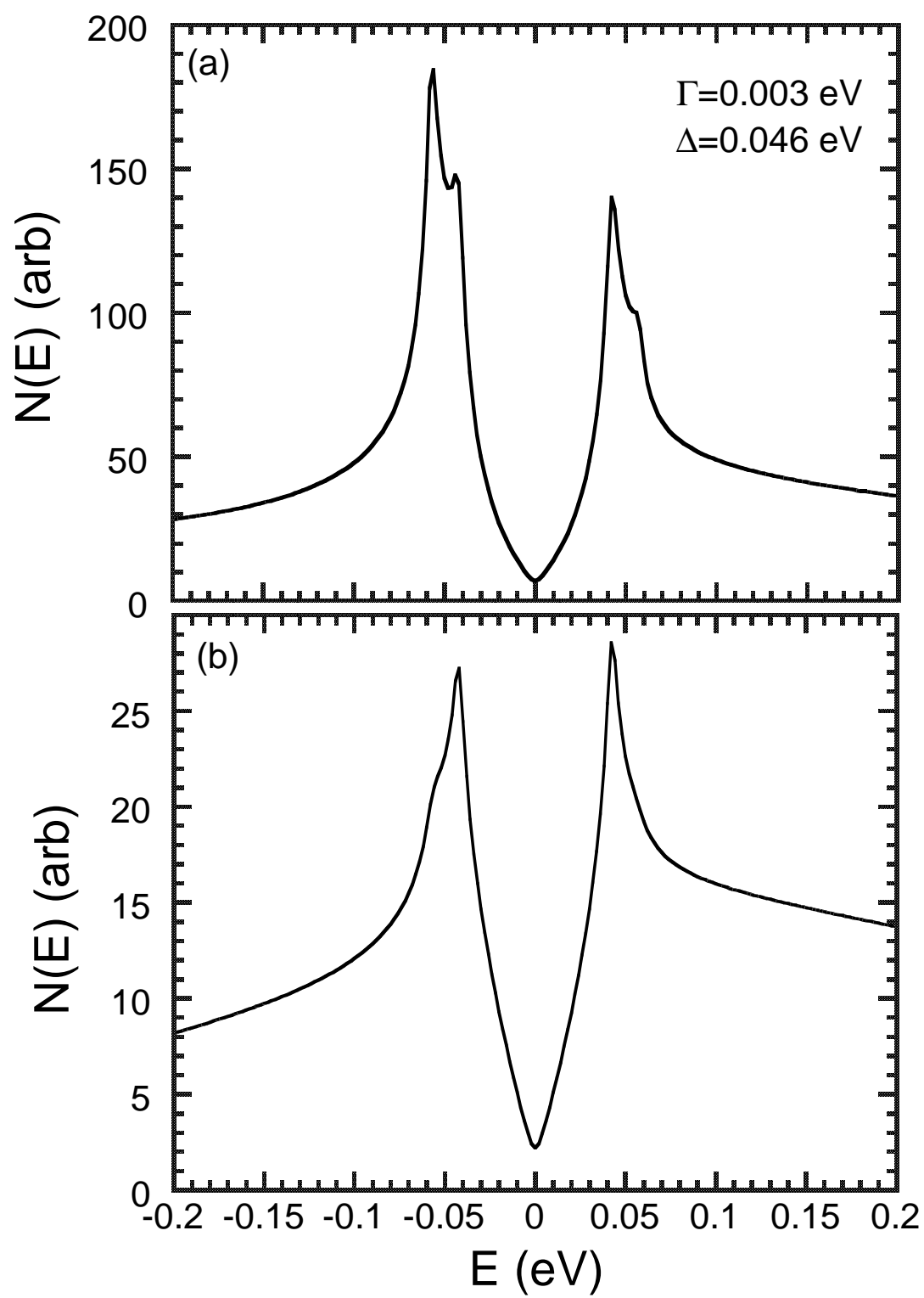


Fig. 5

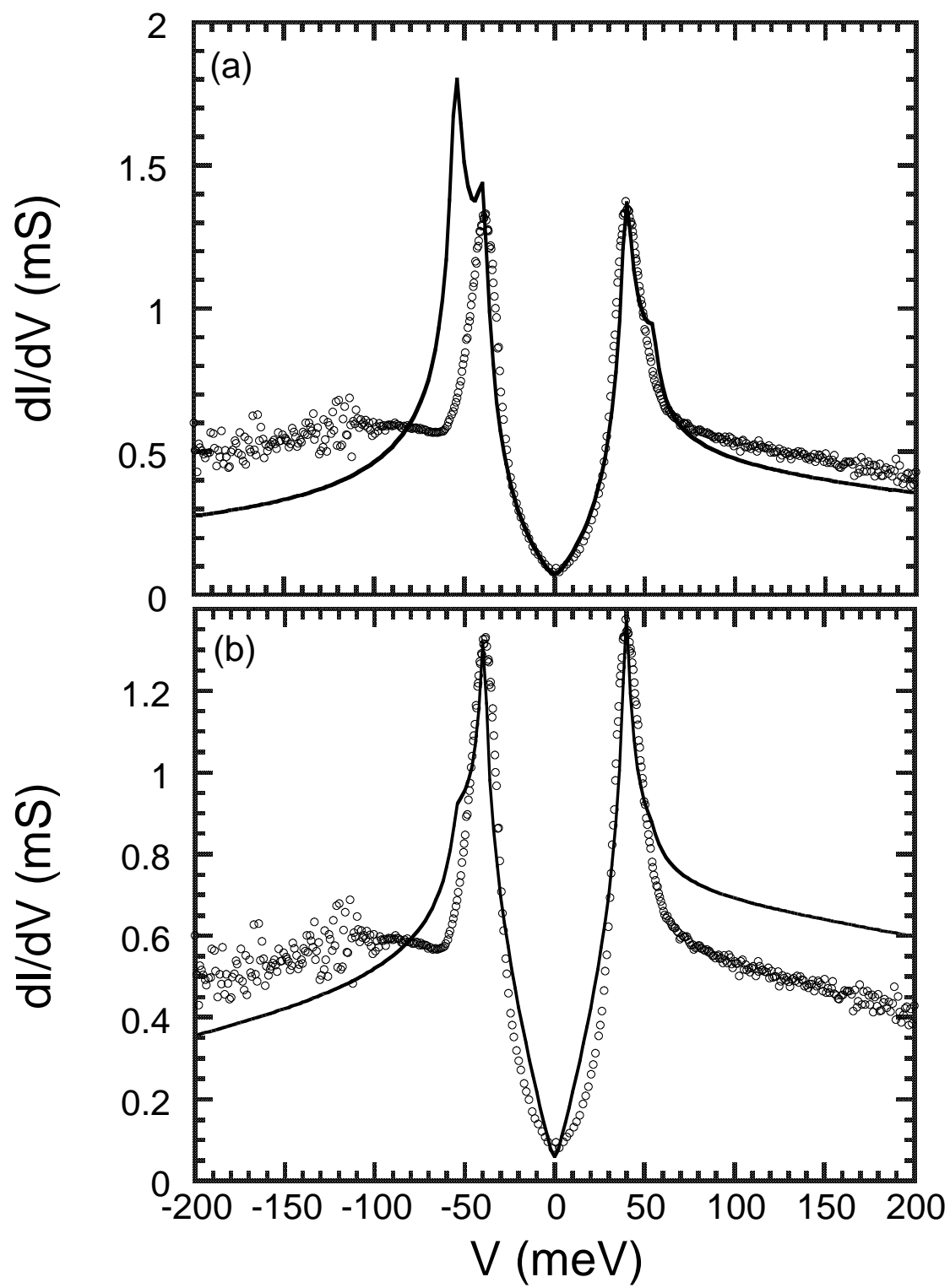


Fig. 6

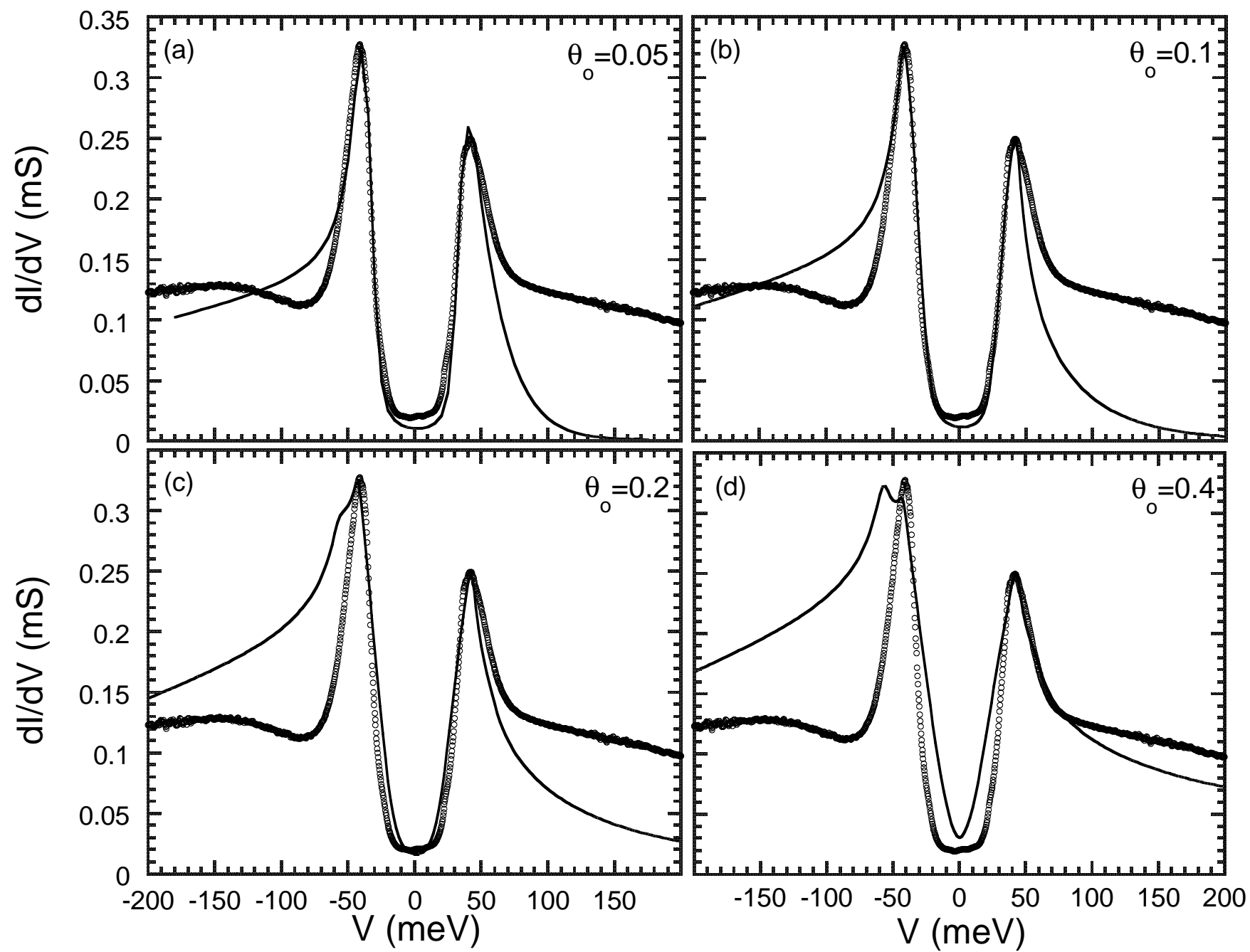


Fig. 7

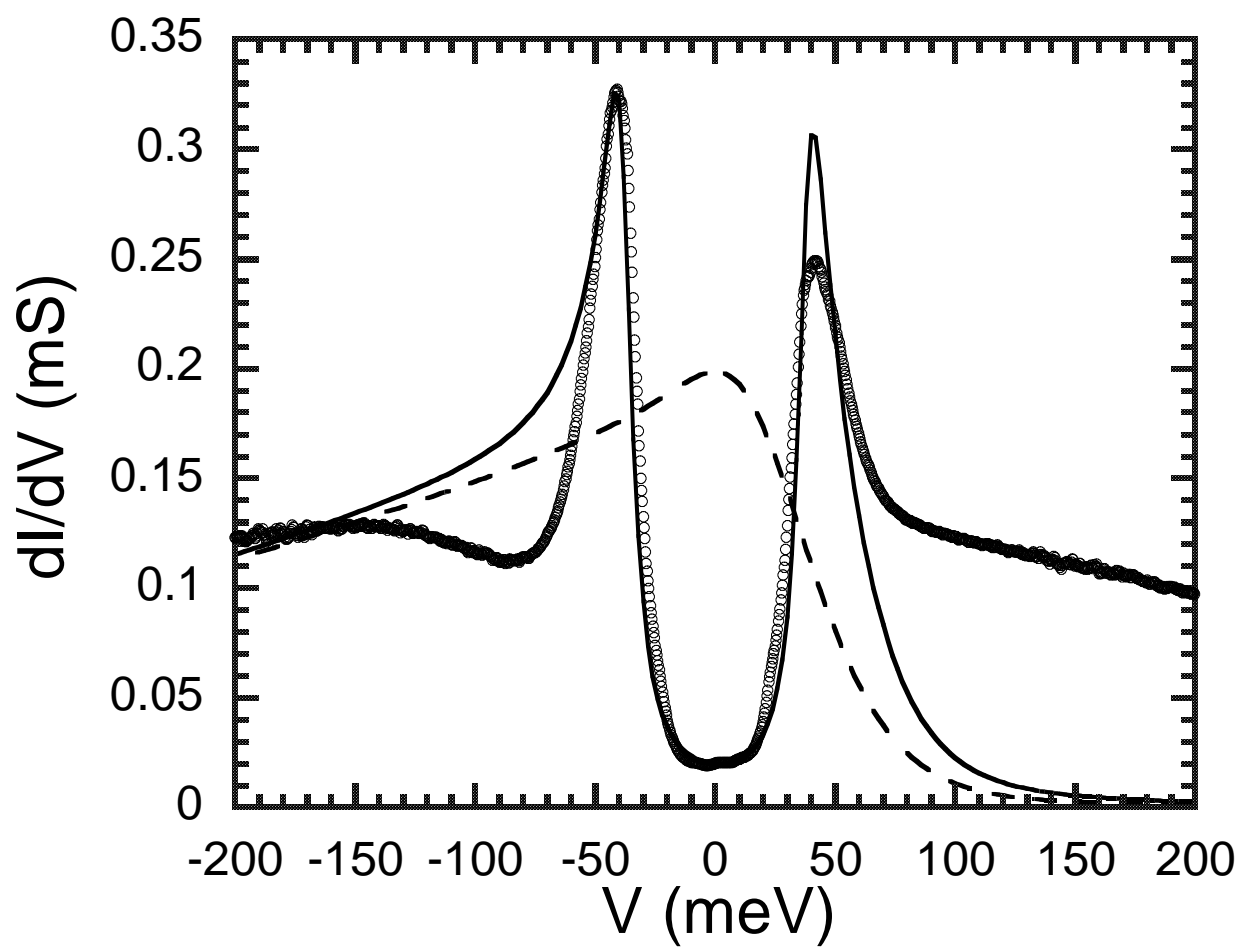


Fig. 8

